## PAPER

Check for updates

# Enhanced ionic conductivity of protonated antiperovskites *via* tuning lattice and rotational dynamics†

Chaohong Guan, Yu Yang, Runxin Ouyang, Huirong Jing, Jieqiong Yan and Hong Zhu [ID] *

The thermodynamically more stable lithium halide hydroxide, $Li_2OHCl$, is experimentally easier to synthesize than $Li_3OCl$. However, the protonated antiperovskite has low ionic conductivity at room temperature due to the limited reorientation of OH anions. Here, density functional theory calculations were performed to determine the stability, elastic properties and Li diffusion of brominated $Li_2OHCl$ ($Li_2(OH)_{0.9}Br_{0.1}Cl$ and $Li_2OHCl_{0.9}Br_{0.1}$). The Br substitution weakens the local bonding interactions and promotes the reorientation of OH anions, thus increasing the ionic conductivities. Based on this, the reorientation of OH anions is further accelerated by substituting Cl with $BH_4$ anions, and this novel protonated antiperovskite exhibits a high ionic conductivity of 2.1 mS cm$^{-1}$ at room temperature. Our work highlights that combining multiple factors, the overall soft lattice and the soft rotation mode of anion groups correlated to Li migrations, can effectively optimize the Li ion conductivity, which might be a universal descriptor to further screen or design other classes of solid-state electrolytes.

## 1. Introduction

The continuously growing need for improving the safety of current aqueous lithium-ion batteries has stimulated intensive work in the field of solid-state electrolytes (SSEs), such as the inorganic SSEs,[1,2] the nonflammability of which guarantees intrinsic safety. In the last few decades, many inorganic SSEs, such as sulfide composites $Li_{10}MP_2S_{12}$ (M denotes Ge, Sn or Si)[3–5] and lithium-rich antiperovskites (APs),[6] have been developed and exhibit ionic conductivities comparable to or even exceeding those of traditional liquid electrolytes. $Li_3OCl$, as one of the most interesting AP materials, has a high ionic conductivity >1 mS cm$^{-1}$ at room temperature and high stability toward Li metal anodes.[7,8] However, in experiments, the intrinsic hygroscopic properties of $Li_3OCl$ severely obstruct the successful synthesis of pure $Li_3OCl$, resulting in the formation of the protonated APs ($Li_2OHCl$). The thermodynamically more stable lithium halide hydroxides[9–11] exhibit high stability with Li metal anodes and are attracting much attention from researchers.

However, the lithium halide hydroxides, such as $Li_2OHCl$, $Li_5(OH)_2Cl_3$, $Li_4(OH)_3Br$, and $Li_5(OH)_4I$, have been reported to exhibit low ionic conductivity at room temperature ($10^{-6}$–$10^{-4}$ mS cm$^{-1}$),[10,12–15] and how to break the limitation of their low lithium-ion diffusion dynamics is still a large challenge.[16] Fortunately, after 1981, the determined high-temperature stabilized cubic $Li_2OHCl$ with the space group of $Pm\bar{3}m$ exhibits higher ionic conductivity (~0.1 mS cm$^{-1}$) compared to the room-temperature orthorhombic $Li_2OHCl$ (~4.3 × $10^{-5}$ mS cm$^{-1}$).[10,13] Previous studies have reported that the high conductivity of $Li_2OHCl$ at high temperature is attributed to the reorientation of the OH groups in the cubic phase.[17,18] Instead, at RT, the formed orthorhombic phase limits the correlated dynamics between lithium ions and OH groups, resulting in low ionic conductivity.[19] To improve the ionic conductivity at low temperature, halogen anion substitutions have been explored to obtain the stable cubic phase with enhanced ionic conductivity compared to the $Li_2OHCl$ at room temperature,[11,14,20–22] which was attributed to the weaker Coulomb interactions and the structural distortion triggered by the different radius of halogen anions, such as $Li_2OHBr_{1-n}X_n$ (X = Cl, I), $Li_2(OH)_{1-n}F_nCl$, $Li_2OHF_n$-$Cl_{1-n}$. The stable cubic $Li_2(OH)_{0.9}F_{0.1}Cl$ exhibits an ionic conductivity of 0.035 mS cm$^{-1}$ compared to the high-temperature cubic $Li_2OHCl$ (0.03 mS cm$^{-1}$) due to the fast rotation of OH anions.[11,23] Recently, Lee *et al.*[21] attempted to partially substitute OH groups by Br and synthesized the $Li_2(OH)_{0.9}Br_{0.1}Cl$ (0.121 mS cm$^{-1}$), which exhibits the highest conductivity of the lithium halide hydroxides at RT. Besides, Mauro and co-workers[24] comprehensively studied the Li-ion conductivity in $Li_2OHCl_{1-x}Br_x$ ($x$ = 0–1) antiperovskites,

*University of Michigan–Shanghai Jiao Tong University Joint Institute, Shanghai Jiao Tong University, Shanghai 200240, China. E-mail: hong.zhu@sjtu.edu.cn*

† Electronic supplementary information (ESI) available: The method of searching ground-state structures, evaluating the phase stability, electrochemical stability, and elastic moduli of the electrolytes and the detailed analysis of the trajectories from the AIMD simulations. See DOI: https://doi.org/10.1039/d2ta08307h

and identified that $Li_2OHCl_{0.9}Br_{0.1}$ exhibits a high conductivity of 0.0025 mS cm$^{-1}$. Hence, among the halogen anions, the Br anion appears to be an effective substituent to improve the ionic conductivity of the lithium halide hydroxides, which is also dependent on the substitution site. Meanwhile, some questions that arise are what is the origin of the high conductivity for the brominated antiperovskites, and will the paddlewheel effects contribute to the Li ion conductivity in the protonated APs? Importantly, recent studies based on $Li_2OHCl$ electrolytes focus on the explanation of the low ionic conductivity of $Li_2OHCl$ at room temperature and how to form cubic $Li_2OHCl$ at room temperature under different experimental conditions; the insights of conduction mechanisms in lithium halide hydroxides to guide the further enhancement of ionic conductivities are lacking.

Thus, in this work, brominated antiperovskites ($Li_2(OH)_{0.9}Br_{0.1}Cl$ and $Li_2OHCl_{0.9}Br_{0.1}$) were systematically studied by density functional theory (DFT) calculations to assess the influences of Br substitution on chemical and electrochemical stability, and deformability. Most importantly, the underlying mechanism for the enhanced Li ion diffusion in the brominated antiperovskites was highlighted, and the mean square distance (MSD), hopping times of Li ions, radial distribution function (RDF), phonon DOS and angular autocorrelation function were analyzed based on the *ab initio* molecular dynamics (AIMD) simulations. In addition, $Li_2OHBH_4$ was designed, which exhibits higher ionic conductivity attributed to the strengthened paddlewheel effect. From the above results, the structure–property correlations were extracted, suggesting the importance of combining multiple factors for the fast Li-ion migration, including the overall lattice softening and special soft anion rotational modes correlated to Li migration, which should be considered for developing and screening novel fast ionic conductors.

## 2. Computational methods

Spin-polarized first-principles calculations were implemented using the Vienna *ab initio* simulation package (VASP)[25,26] with an energy cutoff of 520 eV, and the Perdew–Burke–Ernzerhof (PBE) functional within the generalized gradient approximation (GGA) was adopted to address the exchange–correlation interactions.[27,28] The $2 \times 2 \times 2$ $k$-point mesh was adopted for the Brillouin zone sampling for the $3 \times 3 \times 3$ supercell of studied systems ($Li_2(OH)_{0.9}Br_{0.1}Cl$, $Li_2OHCl_{0.9}Br_{0.1}$, and $Li_2OHCl$). The hybrid functional (HSE06)[29] was used to calculate the band gaps. In addition, the pymatgen package[30] was adopted for building initial structures and analyzing the electrochemical stability. To obtain the stable structures of $Li_2(OH)_{0.9}Br_{0.1}Cl$, $Li_2OHCl_{0.9}Br_{0.1}$, and $Li_2OHCl$ with the lowest energy, 2925 and 20 000 random configurations were created to pick the most stable structure of brominated APs and $Li_2OHCl$, respectively. The detailed process is shown in the ESI†. During the structural optimization, all atoms were relaxed until the convergence criteria of energy ($1 \times 10^{-6}$ eV) and force (0.01 eV Å$^{-1}$) were reached.

Based on the convex hull, the phase diagrams were generated to reveal the phase stability of $Li_2(OH)_{0.9}Br_{0.1}Cl$, $Li_2OHCl_{0.9}Br_{0.1}$ and $Li_2OHCl$ in the compositional space of brominated lithium halide hydroxides. To evaluate the electrochemical stability, the grand potential phase diagram[31] was plotted to show the electrochemical window. For the calculation of elastic moduli (including bulk, shear, and Young's moduli), the Voigt–Reuss–Hill approximation[32] was used. In addition, the AIMD simulations were conducted to study the ionic conductivity, and the ion motion trajectories were further extracted to analyze the conduction mechanism of Li ions (see Section 2 of the ESI† for details).

## 3. Results

### 3.1 Ground-state structure and synthesizability

According to the procedure stated in the method and Section S1,† the ground-state structures of $Li_2(OH)_{0.9}Br_{0.1}Cl$, $Li_2OHCl_{0.9}Br_{0.1}$, and $Li_2OHCl$ were obtained, respectively. As shown in Fig. S1a,† the Li sites and H sites of unrelaxed cubic $Li_2OHCl$ are partially occupied and the OH groups point toward the Cl sites, the corresponding lattice constant of this unrelaxed unit cell is $a = b = c = 3.91$ Å.[20] However, after structural optimization, the cubic phase will transform into the tetragonal phase (Fig. S1b†) with a lattice constant of $a = c > b$ (Table S1†). Interestingly, the OH groups are ordered and point to the Li vacancy sites ($V'_{Li}$); this phenomenon is well consistent with the previous studies of Dawson *et al.*[9] and Effat *et al.*[20] In addition, the ground-state configurations of $Li_2(OH)_{0.9}Br_{0.1}Cl$ and $Li_2OHCl_{0.9}Br_{0.1}$ are shown in Fig. 1 and the detailed lattice information is presented in Table S2.† The results of the two brominated compounds show that the alignment of OH groups is similar to $Li_2OHCl$, and the structure is pseudocubic, which facilitates the migration of Li ions, see Section 3.4.†

To reveal the synthesizability of $Li_2OHCl$, $Li_2(OH)_{0.9}Br_{0.1}Cl$, and $Li_2OHBr_{0.1}Cl_{0.9}$ with respect to that of $Li_3OCl$, the reaction energy ($\Delta E$) is defined as the energy difference between products and reactants. According to ref. 7 and 10, $Li_3OCl$ and $Li_2OHCl$ can be synthesized according to the equations:

$$2LiOH + LiCl = Li_3OCl + H_2O \tag{1}$$

$$LiOH + LiCl = Li_2OHCl \tag{2}$$
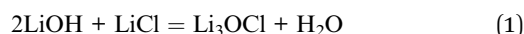
The calculated $\Delta E$s are 1.51 eV and 0.33 eV for eqn (1) and (2), and the smaller $\Delta E$ of $Li_2OHCl$ indicates that it is easier to synthesize in experiments than $Li_3OCl$. Moreover, as mentioned in the Introduction, the pure $Li_2OHCl$ was synthesized by some groups while the synthesis of pure $Li_3OCl$, to date, is still a challenge. To explain this phenomenon, Dawson *et al.*[9] suggested that the low stability of $Li_3OCl$ in ambient air is due to the following reaction:
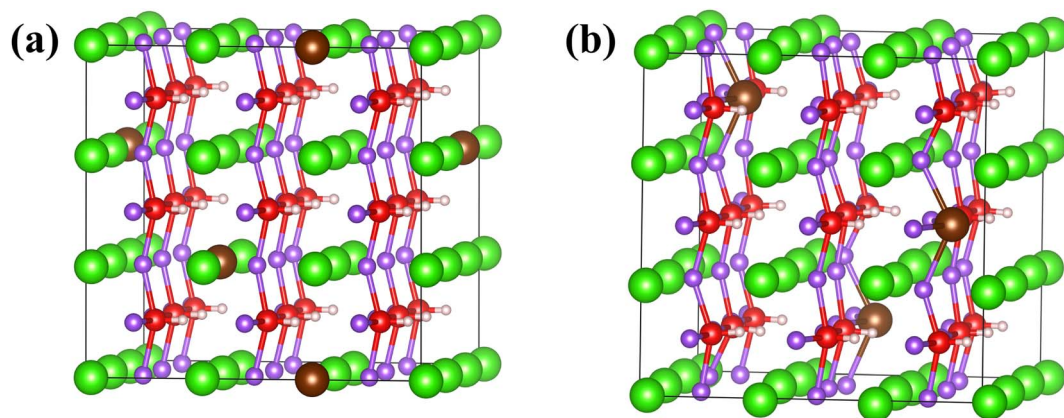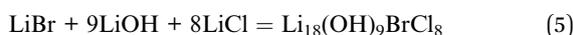
$$Li_3OCl + \frac{1}{2}H_2O = Li_2OHCl + \frac{1}{2}Li_2O \tag{3}$$

**Fig. 1** Ground state structure of (a) $Li_2OHBr_{0.1}Cl_{0.9}$ and (b) $Li_2(OH)_{0.9}Br_{0.1}Cl$. The purple, red, white, green, and brown spheres represent the lithium, oxygen, hydrogen, chlorine, and bromine atoms, respectively.

The $\Delta E$ of eqn (3) in this work is $-0.746$ eV, which is consistent with the reported result by Dawson *et al.* ($-0.74$ eV). Besides, Hanghofer *et al.*[33] proposed that the $Li_4(OH)_3Cl$ impurity phase was formed during the synthesis of $Li_3OCl$ as the following equation shows:

$$Li_3OCl + \frac{1}{2}H_2O = \frac{2}{3}Li_4(OH)_3Cl + \frac{1}{3}Li_2O \qquad (4)$$
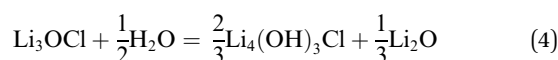
Compared to eqn (3), a more negative $\Delta E$ of eqn (4) ($-1.52$ eV) was calculated, which further validates the experimental phenomenon that producing pure $Li_3OCl$ is challenging.

Regarding the brominated lithium halide hydroxides, the $Li_2OHBr_{0.1}Cl_{0.9}$ and $Li_2(OH)_{0.9}Br_{0.1}Cl$ can be obtained according to following reaction equations:[34]

$$LiBr + 9LiOH + 8LiCl = Li_{18}(OH)_9BrCl_8 \qquad (5)$$

$$LiBr + 8LiOH + 9LiCl = Li_{18}(OH)_8BrCl_9 \qquad (6)$$

The calculated $\Delta E$s of eqn (5) and eqn (6) are $-3.29$ eV and $-2.90$ eV, respectively, indicating the high spontaneous reaction trend and the high synthesizability.

### 3.2 Phase stability and electrochemical stability

The phase diagrams were employed to assess the phase stability of $Li_2OHCl$, $Li_2(OH)_{0.9}Br_{0.1}Cl$, and $Li_2OHBr_{0.1}Cl_{0.9}$. Due to the difficulty of visualization of the Gibbs tetrahedron, the Gibbs-tetrahedron projections of all studied structures are presented.[35] Fig. 2 exhibits the phase diagrams of protonated APs, the corner compositions represent the precursors adopted in the synthesis of protonated APs, whose phase diagrams are shown in Fig. S2.† As presented in Fig. 2a, the $Li_2OHCl$ is metastable (energy above hull is 21 meV per atom) and may decompose into $Li_4(OH)_3Cl$ and LiCl. Hence, some impurities including LiCl or $Li_4(OH)_3Cl$ in the $Li_2OHCl$ samples may be found. However, the previous studies[15,36] did not detect $Li_4(OH)_3Cl$ in the synthesized $Li_2OHCl$, and further experimental study is needed for confirming the properties or synthesis

conditions of $Li_2OHCl$. Fig. 2d and g display the phase diagrams of $Li_{18}(OH)_8BrCl_9$ and $Li_{18}(OH)_9BrCl_8$, respectively. Both brominated lithium halide hydroxides are stable, indicating that the pure phase of $Li_{18}(OH)_9BrCl_8$ and $Li_{18}(OH)_8BrCl_9$ can be obtained in experiments. The temperature-dependent free energies are shown in Fig. S3,† suggesting the high stability of $Li_2(OH)_{0.9}Br_{0.1}Cl$ compared to $Li_2OHCl$.

The electrochemical stability can be characterized by the density of states (DOS) and the grand potential phase diagram (GPPD). For $Li_2OHCl$, the band gap is determined to be 6.65 eV (as displayed in Fig. 2b, corresponding partial density of states is shown in Fig. S4†), in good agreement with the work of Mohammed *et al.* (6.6 V),[20] implying the wide electrochemical window of protonated APs. On the other hand, the GPPD of $Li_2OHCl$ indicates that the reduction reactions occur when the voltage is below 0.45 eV, and the oxidation reactions occur when the voltage is above 3.76 V *vs.* $Li/Li^+$. Compared to other specific SSEs, the electrochemical window of $Li_2OHCl$ is wider than those of the sulfides[37] (such as $Li_3PS_4$, $Li_{10}GeP_2S_{12}$, *etc*), and comparable to those of some oxides[38] or halides,[39] details can be seen in Fig. S5,† which also shows that the protonation of $Li_3OCl$ broadens the electrochemical window from 3 V to 3.31 V, increasing the electrochemical stability of this AP. Furthermore, the related decomposition reactions, as shown in S3.1,† demonstrate the possibility for $Li_2OHCl$ reacting with electrodes to form the solid electrolyte interphase layer (SEI) in the first few cycles, which has wider windows thus preventing the reactions between $Li_2OHCl$ and electrodes under the operational voltage of the $Li_2OHCl$-based battery. For example, Hood *et al.*[10] detected LiCl in the $Li_2OHCl$–Li metal interface, the electrochemical window of this SEI species is about 4.25 V, and this SEI is beneficial to the normal operation of the $Li_2OHCl$-based battery. However, as shown in Fig. 2c, at a voltage above 3.76 V, some non-Li-containing species may be formed, such as $H_3ClO$, $H_7ClO_3$, or $ClO_2$, which exhibit low ionic conductivities, resulting in the deterioration of battery performance. Therefore, preventing the oxidative decomposition of $Li_2OHCl$ is very crucial for the application.
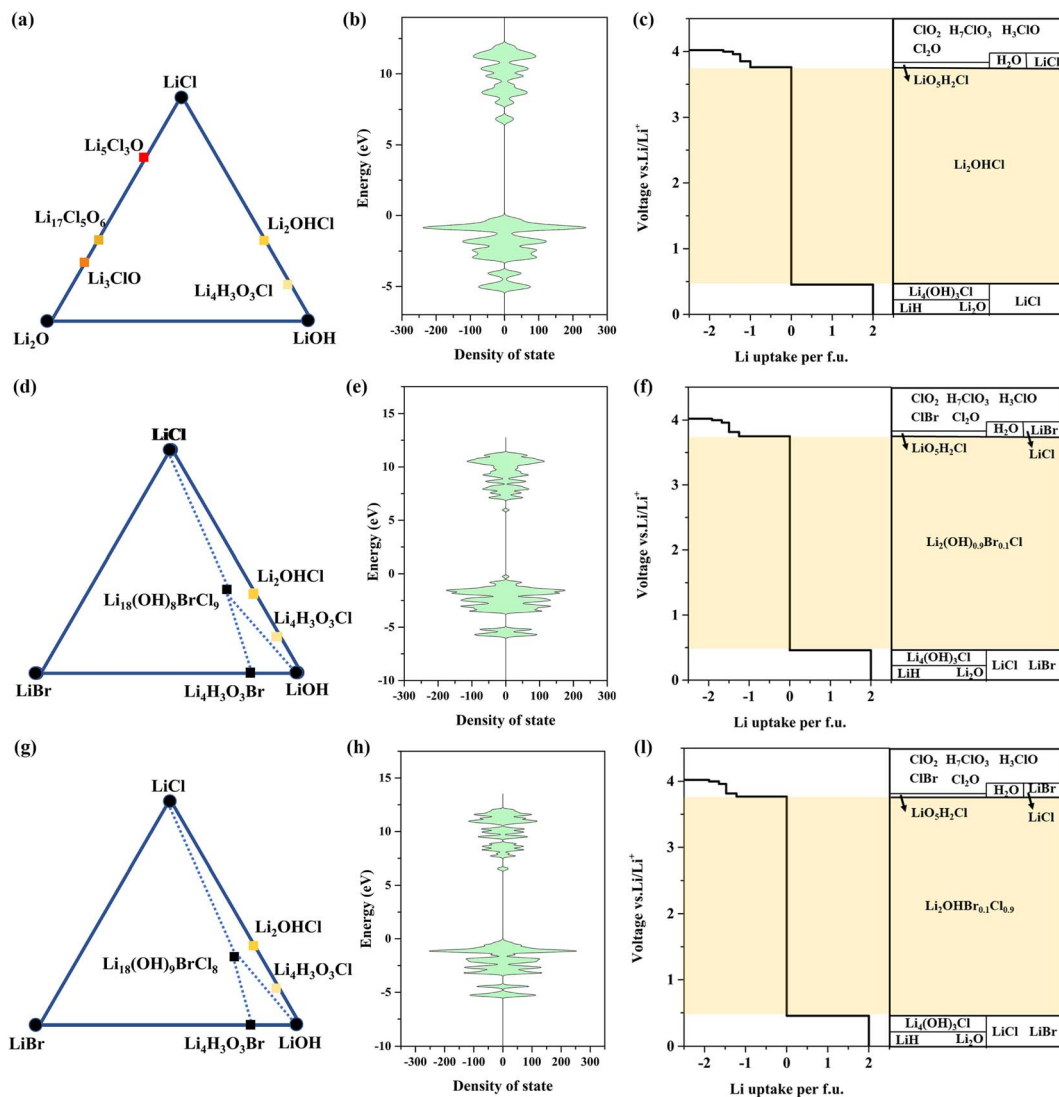
**Fig. 2** The Gibbs–phase–diagram projections for (a) $Li_2OHCl$, (d) $Li_{18}(OH)_9BrCl_8$ and (g) $Li_{18}(OH)_8BrCl_9$. The black dots represent the precursors in the experiment; in addition, the black dots and squares represent stable phases, and the yellow and red squares represent unstable phases with relatively small and large energy above the hull, respectively. The density of states and electrochemical stability windows for (b and c) $Li_2OHCl$ (e and f) $Li_2(OH)_{0.9}Br_{0.1}Cl$ and (h and i) $Li_2OHBr_{0.1}Cl_{0.9}$, respectively.

Fig. 2e, f, h and i show the DOS and GPPD of $Li_2(OH)_{0.9}$-$Br_{0.1}Cl$ and $Li_2OHBr_{0.1}Cl_{0.9}$, respectively; all decomposition reactions are displayed in S3.2 and S3.3.† Obviously, $Li_2(-OH)_{0.9}Br_{0.1}Cl$ and $Li_2OHBr_{0.1}Cl_{0.9}$ exhibit comparable band gaps and electrochemical windows with $Li_2OHCl$, maintaining the high electrochemical stability and low electronic conductivity as $Li_2OHCl$, decreasing the possibility of electronic leakage during battery operation. And the partial density of states also is provided (Fig. S4†), which indicates that the valence band maximum (VBM) of the three studied structures is dominated by the O, Cl, or Br anions, which means O, Cl, or Br anions are the first species to be oxidized at high voltages. And the conduction band minimum (CBM) is mainly dominated by the Li cations, which can be reduced first at low voltages. The large gaps between VBM and CBM provide an upper boundary of electrochemical stabilities. In addition, when the voltage is below 0.46 V (0.456 V), the $Li_2(OH)_{0.9}Br_{0.1}Cl$ and $Li_2OHBr_{0.1}Cl_{0.9}$

decompose into LiBr, LiCl, and other compounds; the formed halides show wider stability windows (3.64 V and 4.23 V for LiBr and LiCl, respectively) than these lithium halide hydroxides. Above 3.76 V (3.77 V), similar to $Li_2OHCl$, some non-Li-containing species will be formed, such as $H_3ClO$, $H_7ClO_3$, ClBr *etc.*, the low lithium conductivities of which degrade the battery performance. These results further confirm that to match with a high-voltage cathode, protective methods are needed to prevent the decomposition of APs.

## 3.3 Elastic properties

The mechanical properties, including bulk modulus (*B*), Young modulus (*E*), and shear modulus (*G*), are also crucial parameters to evaluate the performance of SSEs. The three moduli assess how the SSE responds to volumetric, tensile, and shear stress, hence, which exhibit a deep impact on the cycling

performance,[40] owing to the constructed solid–solid interface between electrolytes and electrodes. Furthermore, as discussed in the previous study, the ductile SSEs are easier to assemble and stacked in the cell.[41] Considering both the factors, the moduli of our studied SSEs were calculated, as displayed in Fig. S6,† and the detailed values are shown in Table S3† and the detailed data of total elastic moduli are listed in Table S4.†

The calculated values of $B$, $E$, and $G$ of $Li_3OCl$ are comparable with the results of Pegolo et al.,[42] and the moduli of protonated and brominated $Li_3OCl$ are relatively less than that of pure $Li_3OCl$, suggesting that protonated and brominated $Li_3OCl$ can tolerate the greater stress originating from the deformation of electrodes and improve the cycling performance. In addition, the Pugh ratios (listed in Table S3,† $G/B$) of $Li_3OCl$ and $Li_2OHCl$ are larger than 0.6 ($G/B < 0.6$ and $G/B > 0.6$ represent the ductility and brittleness of the material,[43] respectively); hence, both SSEs are brittle. Specifically, the values of Pugh ratios of brominated $Li_2OHCl$ are less than 0.6, indicating the ductility of both SSEs, the decreases in the Pugh ratio can be explained from the chemical intuition, confirmed by the Bader analysis[44] (Table S5†), which suggests that the introduction of the Br element decreases the strength of ionic bonds. The electron localization function (ELF) has been calculated to visualize the charge distributions, as shown in Fig. S7.† As indicated by the ELF, the atoms in the three studied structures are separated by a low electron density region, and the electrons are localized around the nucleus, suggesting that the bonds are predominantly ionic. For the OH groups, the O and H atoms were separated by a relatively high electron density region, exhibiting covalent interactions.

### 3.4 Diffusion properties

The AIMD simulations were conducted from 800 to 1200 K to study the ionic diffusion properties of brominated APs, and the obtained Arrhenius plot (and the activation energies) are shown in Fig. 3a. For $Li_2OHCl$ SSE, the derived activation energy and ion conductivity at 373 K are 0.46 eV and 0.19 mS cm$^{-1}$, which are comparable with the reported values of Hood et al.[10] ($1 \times 10^{-4}$ S cm$^{-1}$). And Mohammed et al.[20] reported that the activation energy and conductivity of $Li_2OHCl$ are 0.48 eV and 0.16 mS cm$^{-1}$ at 373 K, which are well consistent with our results. In addition, the anion substitution with bromine can improve the ionic conductivity of $Li_2OHCl$ SSE; the corresponding activation energies are 0.30, 0.41, and 0.46 eV ($Li_2(OH)_{0.9}Br_{0.1}Cl < Li_2OHBr_{0.1}Cl_{0.9} < Li_2OHCl$). Specifically, the Li-ion conductivity of $Li_2(OH)_{0.9}Br_{0.1}Cl$ is higher than that of $Li_2OHCl$ and $Li_2OHBr_{0.1}Cl_{0.9}$, revealing that it is more effective to improve ionic conductivity by substituting the OH group with the bromine element. Besides, we assess the diffusion kinetics of Li ions for two diffusion paths (Fig. S8a,† path1 and path2) by the climbing image nudged-elastic-band method (CI-NEB). Also, the activation energy barriers along each path in the three structures follow the order of $Li_2(OH)_{0.9}Br_{0.1}Cl < Li_2OHBr_{0.1}Cl_{0.9} < Li_2OHCl$, indicating the faster ionic migration in $Li_2(OH)_{0.9}Br_{0.1}Cl$, in agreement with our AIMD simulations.

To probe the ionic migration process, the mean square displacements (MSDs) were extracted from the AIMD simulations, as plotted in Fig. 3b–d. As reported in previous studies,[11] there is a debate whether these AP materials are fast proton conductors. Our AIMD results show that the MSDs of protons nearly remain constant with time, and the MSDs are around 2 Å$^2$, which is far less than the distance of the O–O pair (3.91 Å)[17] in these APs. Hence, the proton migration via the Grotthuss mechanism[45] does not occur in both brominated APs considered in our work. Fig. 3e and f support this conclusion that the protons only move around the oxygen atom while any long-range migration is not found. The studies of Dawson et al.[9] also suggest the rotation of OH groups in $Li_2OHCl$, which has
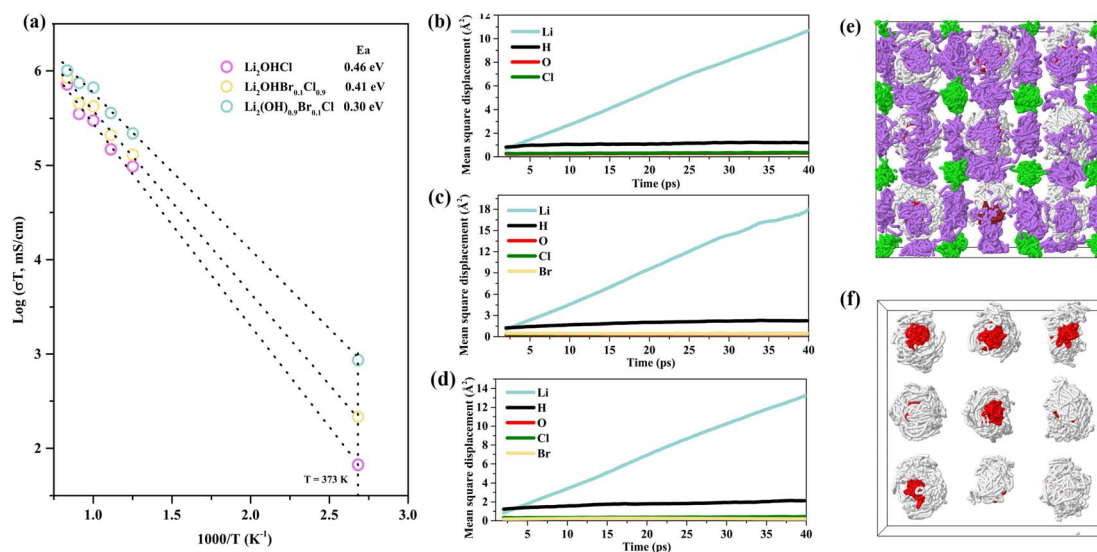


**Fig. 3** (a) The derived Arrhenius plots of the $Li_2OHCl$, $Li_2(OH)_{0.9}Br_{0.1}Cl$, and $Li_2OHBr_{0.1}Cl_{0.9}$. (b–d) The mean square displacement (MSD) for $Li_2OHCl$, $Li_2(OH)_{0.9}Br_{0.1}Cl$, and $Li_2OHBr_{0.1}Cl_{0.9}$ at 800 K, respectively. (e) and (f) The ion migration trajectories in $Li_2(OH)_{0.9}Br_{0.1}Cl$ during the AIMD simulations. The purple, green, red, and white represent the trajectories of lithium, chlorine, oxygen, and hydrogen, respectively.

significant effects on the migration of lithium. Here, we note that the Br substitution increases the MSDs of H atoms but does not affect those of O atoms, which may indicate the enhanced rotation of OH groups, which will be further discussed in the following.

## 4. Discussion

To further understand how brominating the sublattice of $Li_2OHCl$ ($Li_2(OH)_{0.9}Br_{0.1}Cl$ and $Li_2OHBr_{0.1}Cl_{0.9}$) influences the dynamics of lithium and OH groups, the AIMD results were further analyzed, and the related analytical methods are discussed in the ESI.† To evaluate the Li ion mobility in $Li_2OHCl$ and brominated APs, the times of Li ion hops at 800 K were calculated as displayed in Fig. 4. Obviously, brominated APs show more hopping times compared to $Li_2OHCl$. As described in Section S4,† the individual and concurrent hops were counted to reveal the diffusion mechanisms. The 2-dimensional schematics of the Li hops are shown in Fig. 4a, and the individual hop represents a direct jump from a Li site to a vacant site, and the concurrent hop represents concerted migration of two Li atoms.

Though both hops have contributions to the Li ion diffusion (Fig. 4b), the individual hops are the main jumping style for Li ions in the three APs. However, the substitutions of OH group or chlorine element by bromine in $Li_2OHCl$ enhance the total number and the percentage of concurrent hops (Fig. 4c), and the $Li_2(OH)_{0.9}Br_{0.1}Cl$ exhibits the highest percentage of concurrent events as well as the highest ionic conductivity in the three APs. To shed light on the local diffusion bottleneck, the interactions between Li and anions (Cl, O, and Br) were analyzed based on the AIMD simulations. Ions-pair distances were measured for reflecting this interaction, and the larger distance facilitates the diffusion of Li ions. Fig. 4d–f display the radial distribution function (RDF) *versus* ion-pair distance in $Li_2OHCl$, $Li_2(OH)_{0.9}Br_{0.1}Cl$, and $Li_2OHBr_{0.1}Cl_{0.9}$, respectively. The locations of the first peaks of Li–Cl and Li–O pairs remain almost constant in these APs, with radial distances around 2.38 Å and 1.95 Å, respectively. However for the Li–Br pair, the peaks shift to the larger radial distance, demonstrating the weaker Coulomb interaction between Li and Br compared to the Li–Cl pair. In addition, previous studies have reported that local structural distortion can effectively improve ionic conductivity.[46] The large ionic size differences between anions (Br, Cl, and OH, whose ionic radii are 196, 181, and 140 pm, respectively)[47] result in the local structural distortion in the brominated electrolytes, which may be responsible for the increasing mobility of Li ions in $Li_2(OH)_{0.9}Br_{0.1}Cl$ and $Li_2OHBr_{0.1}Cl_{0.9}$.
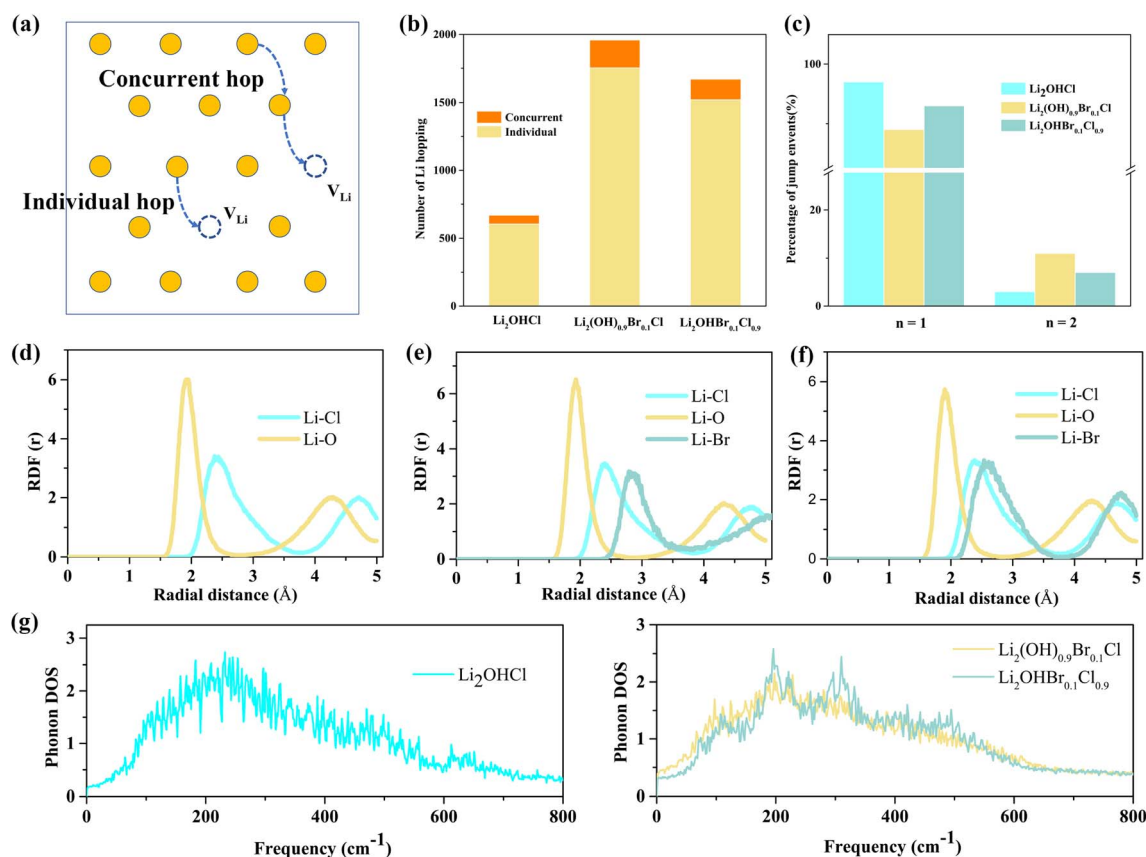


Fig. 4 (a) The 2-dimensional schematics for describing the individual hop and the concurrent hop for Li ions (b) hopping number of Li in the three $Li_2OHCl$-based APs at 800 K during the last 70 ps. The light yellow and orange represent the individual and concurrent hops, respectively. (c) The percentage of jump events with $n = 1$ or $n = 2$, see S5 in the ESI.† (d–f) Radial distribution functions (RDF) for $Li_2OHCl$, $Li_2(OH)_{0.9}Br_{0.1}Cl$ and $Li_2OHBr_{0.1}Cl_{0.9}$ SSEs, respectively. (g) The phonon DOS for the three SSEs.

Attributed to the smaller radius of the OH group than Cl, the local distortion is more significant in $Li_2(OH)_{0.9}Br_{0.1}Cl$ than in $Li_2OHBr_{0.1}Cl_{0.9}$. Moreover, the local diffusion channels of Li nearby the Br atoms will be widened. The RDFs greatly explain this result that the greater Li–Br radial distance in $Li_2(OH)_{0.9}Br_{0.1}Cl$ represents the greater local distortion and the weaker bonding, compared to $Li_2OHBr_{0.1}Cl_{0.9}$.

To improve ionic conductivity, great efforts recently have been made on the lattice dynamics by softening the lattices.[48] It has been reported that the softer lattice usually facilitates Li migration and leads to the low energy barriers of mobile ions and high ionic conductivity. The average vibrational frequencies for materials normally have been adopted to describe the lattice dynamics.[49] In this work, the phonon spectra were calculated by a Fourier transform of the autocorrelation function based on the AIMD simulations at 800 K to reveal the behaviors of lattice dynamics in the three APs, as shown in Fig. 4g. Compared with $Li_2OHCl$, the peaks of phonon DOS for the brominated electrolytes shift to a lower frequency and the calculated phonon band centers of $Li_2OHCl$, $Li_2(OH)_{0.9}Br_{0.1}Cl$ and $Li_2OHBr_{0.1}Cl_{0.9}$ are 350.6 cm$^{-1}$, 287.82 cm$^{-1}$, and 319.95 cm$^{-1}$, respectively, indicating the softening of the sublattice with the introduction of bromine. In general, the Br anion helps to form softer bonding and enhance the jump times, which also contributes to the high ionic conductivity in brominated $Li_2OHCl$.

As indicated in the Introduction, the significant connection between the mobility of Li ions and the rotation of OH groups is a critical factor for the fast ionic conductivity of the $Li_2OHCl$-based SSEs; the anion rotation also can be found in other superionic conductors.[50] This connection can be characterized by the angular autocorrelation function (see S4†), as shown in Fig. 5a, which assesses the change of OH group rotation mobility with the substitution of bromine. The superionic $Li_2(OH)_{0.9}Br_{0.1}Cl$ exhibits faster anion rotation than the relatively less diffusive systems, $Li_2OHCl$ and $Li_2OHBr_{0.1}Cl_{0.9}$, which is well consistent with the change of ionic conductivity, suggesting the strong correlation between the higher ionic conductivity and the anion rotation mobility. Consistently, the OH anions in $Li_2(OH)_{0.9}Br_{0.1}Cl$ feature dispersive and disordered rotation with changed angles $\theta$ and $\Phi$ (definition is displayed in Fig. S8†), demonstrating the soft reorientation dynamics of OH anions. In addition, possible interactions between OH groups and lithium diffusion were further studied in Fig. 5b, which displays the vibrational spectrum (phonon DOS) of OH groups in the three $Li_2OHCl$-based SSEs, helping to identify the specific vibrational modes in particular frequency regimes. Combining the results of Fig. 4g, the significant vibrational modes overlap in the low-frequency regime (corresponding to the rotational modes of OH groups and Li ion migration) is found, indicating the possible momentum transfer between the dynamics of OH groups and the lithium
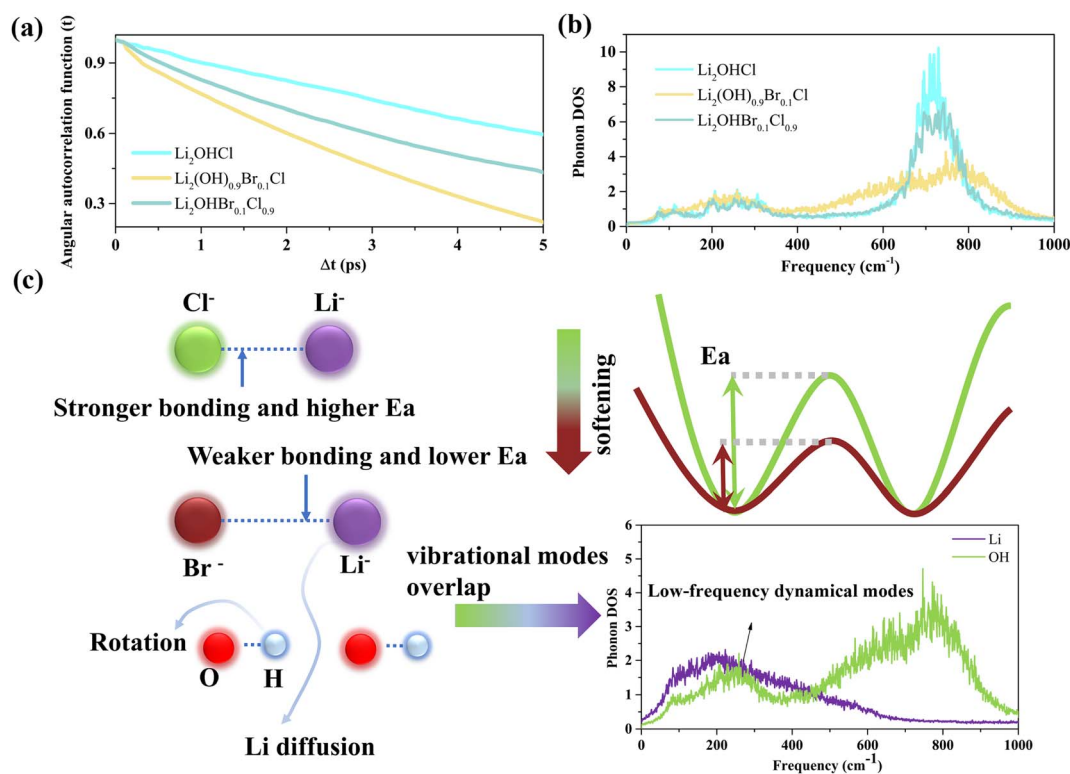


**Fig. 5** To assess the mobility of anion rotation, the (a) angular autocorrelation function and (b) the OH group vibrational spectrum (phonon DOS) of $Li_2OHCl$, $Li_2(OH)_{0.9}Br_{0.1}Cl$, and $Li_2OHBr_{0.1}Cl_{0.9}$ SSEs are calculated based on the AIMD simulations. (c) Schematic of the influences of lattice softening and OH rotation on the activation energy of ionic diffusion, the phonon DOS displays the overlapped low-frequency dynamical modes (soft modes) of $Li_2(OH)_{0.9}Br_{0.1}Cl$.

vibration precursor to hopping events (paddlewheel effect), which accelerates the diffusive dynamics of Li ions.

The high ionic conductivity is intrinsically associated with the distribution of energy landscape, and all of the facts discussed in the above contents can be considered as the main factors to flatten the local energy landscape and decrease the activation energy ($E_a$). As illustrated in Fig. 5c, the lower electronegativity of Br $vs.$ Cl results in the weaker bonding interactions (coulombic force) between Br and diffusive lithium ions, and the lattice softening facilitates the mobility of lithium and the decreased activation energy. Notably, the coulombic inductive effects have been reported in $Li_{10}Ge_{1-x}Sn_xP_2S_{12}$, in which the stronger $Ge^{4+}-S^{2-}$ bonding leads to the weaker coulombic interaction between $Li^+$ and $S^{2-}$ and higher ionic conductivity.[3] In addition, the soft dynamical modes can effectively fluctuate the energy landscape, which may assist the ion diffusion.[51] For the $Li_2OHCl$-based SSEs, the soft modes stem from the rotation of OH groups (Fig. 5c), which can alter the local symmetry and improve the ionic diffusion. Specifically, the $Li_2(OH)_{0.9}Br_{0.1}Cl$ has the fastest rotational dynamics of OH groups and shows the lowest activation energy, the possible reason may be the lower concentration of OH groups compared to the $Li_2OHBr_{0.1}Cl_{0.9}$, which provides enough space for the effective rotation of OH groups and strengthens the paddlewheel effect. Many previous studies[52,53] have reported a similar connection between ionic diffusion and the soft rotation modes in superionic conductors for enhancing ionic conductivity. For example, in $Li_6POS_4(SH)$ and $Li_{6.25}PS_{5.25}(BH_4)_{0.75}$, the high rotational degrees of freedom of $SH^-$ and $BH_4^-$ contribute to the extremely high ionic conductivities at room temperature ($\sigma_{RT} = 82$ mS cm$^{-1}$ and 177 mS cm$^{-1}$ for $Li_6POS_4(SH)$ and $Li_{6.25}PS_{5.25}(BH_4)_{0.75}$, respectively).[54] However recent work indicates that the weak interaction between Li and $BH_4$ contributes to the high ionic conductivity of $Li_{5.91}PS_{4.91}(BH_4)_{1.09}$.[55] Therefore, further study should be conducted to confirm the structural or dynamics features for the paddlewheel effect.

As illustrated in Fig. 5c, the soft lattice and rotational modes can be used to optimize the ionic conductivities of lithium halide hydroxide SSEs, as well as to explore other similar SSEs. For instance, lattice softening can be realized by reducing the cation–anion interactions in ionic conductors (low electronegativity difference). Previous studies[17,20,21] have confirmed the important role of halogen substitution in the cation–anion interactions, while the periodic table limits the number of available halogens. Therefore, superhalogens[54,55] (such as $BH_4^-$ and $AlH_4^-$) have been used to replace halogens (as argyrodite-type SSE, $Li_{6.25}PS_{5.25}(BH_4)_{0.75}$) for avoiding the limitation mentioned above, which may exhibit the lower electronegativity compared to halogens and display weak cation–anion interactions. Yet these interactions must be significant enough to ensure the stability of conductors at ambition temperatures, for which the balance between stability and low activation energies, therefore, needs to be considered. It should be noted that a softer lattice does not always guarantee a higher ionic conductivity.[56] For the soft rotational modes, the introduction of anion clusters with rotational freedom is an effective strategy to help Li diffusion. The suitable type and concentration of anion clusters should be modulated for the high rotational degrees of freedom. Nevertheless, the occurred time scale of the energy landscape fluctuated by rotational modes is a critical factor for assisting the diffusion of cations. If the fluctuation occurs too fast, the instantaneous perturbations are not likely to drive the local diffusion of cations, which only see the mean-field effect. If the fluctuation occurs too slow, the cations will see an unchanged potential and this fluctuation cannot be exploited to escape possible local-minimum traps for enhanced diffusion of cations.[51] Although substitution reactions can effectively tune this time scale, the detailed methods for controlling the time scale should be further studied. Moreover, the too weak or too strong anion–cation interaction could make the facile anion rotation ineffectively; we therefore indicate that multiple factors determine the superionic feature of SSEs.

To further encourage the lithium hopping as well as the paddlewheel effect, a novel protonated antiperovskite was designed by substituting the Cl with $BH_4$ anions, which could have weaker coulombic interaction with Li and spontaneous rotation. As shown in Fig. S10a,† the structure is pseudocubic, which exhibits low activation energy (0.29 eV) and high ionic conductivity (2.1 mS cm$^{-1}$) at room temperature (Fig. S10b†). The dispersive and disordered rotation of OH anions with changed angles $\theta$ and $\Phi$ suggests high rotational freedom (Fig. S10b†), which contributes to fast migration of Li ions. In addition, the enhanced rotational dynamics of anions (including the OH and $BH_4$ anions) compared to $Li_2(OH)_{0.9}Br_{0.1}Cl$ (Fig. S10b†) and the overlapped vibrational modes in the low-frequency regime (Fig. S11,† corresponding to the rotational modes of OH, $BH_4$ anions and Li ions migration) imply the strengthened paddlewheel effect. Hence, to enhance the superionic performance, we suggest that multiple factors should be considered simultaneously, such as the soft overall lattice (e.g., with low coulombic force) and the soft rotation modes (e.g., anion rotation modes correlated to Li migration), which can be considered as a descriptor to design novel SSEs. But what kind of solid electrolytes could be tuned through such multiple factors in an effective way still needs further investigation.

## 5. Conclusion

The phase and electrochemical stabilities, mechanical properties, and ionic diffusion for $Li_2OHCl$-based solid-state electrolytes ($Li_2OHCl$, $Li_2(OH)_{0.9}Br_{0.1}Cl$, and $Li_2OHBr_{0.1}Cl_{0.9}$) had been comprehensively studied to explore the influences of bromination by density functional theory and AIMD simulations. Specifically, the diffusion mechanisms were deeply analyzed based on the ion diffusion trajectories of AIMD simulations. The results suggest that it is easier to synthesize $Li_2OHCl$-based SSEs than $Li_3OCl$, since the former have smaller reaction energies. Different from the metastable structures of $Li_3OCl$ and $Li_2OHCl$, $Li_2(OH)_{0.9}Br_{0.1}Cl$ and $Li_2OHBr_{0.1}Cl_{0.9}$ are stable with the negative formation energies, which suggests that the pure $Li_2(OH)_{0.9}Br_{0.1}Cl$ and $Li_2OHBr_{0.1}Cl_{0.9}$ can be synthesized easily. Furthermore, the introduction of bromine not only facilitates the voltage tolerance of both electrolytes and shows wider

electrochemical windows, but also decreases the values of moduli so that the protonated and brominated $Li_3OCl$ can tolerate the greater stress originating from the deformation of electrodes and improve the cycling performance. Interestingly, brominated $Li_2OHCl$ exhibit higher conductivities than $Li_2OHCl$, and $Li_2(OH)_{0.9}Br_{0.1}Cl$ exhibits the highest conductivity. The high ionic conductivities stem from the weaker bonding interactions (the soft overall lattice dynamics) and the soft rotation modes of OH groups. In addition, a novel protonated antiperovskite was designed by substituting the Cl with $BH_4$ anions and shows higher ionic conductivity compared to $Li_2(OH)_{0.9}Br_{0.1}Cl$, which is attributed to the strengthened paddle-wheel effect. This work highlights the correlations between lattice dynamics and ionic conductivity, suggesting that it is more effective for optimizing ionic conductivity by softening the whole lattice as well as the rotation mode of anion groups. Such multiple factors also can be used to screen or design other classes of SSEs.

## Conflicts of interest

There are no conflicts to declare.

## Acknowledgements

## References

1 C. Yu, F. Zhao, J. Luo, L. Zhang and X. Sun, Recent development of lithium argyrodite solid-state electrolytes for solid-state batteries: Synthesis, structure, stability and dynamics, *Nano Energy*, 2021, **83**, 105858.

2 S. Abouali, C.-H. Yim, A. Merati, Y. Abu-Lebdeh and V. Thangadurai, Garnet-Based Solid-State Li Batteries: From Materials Design to Battery Architecture, *ACS Energy Lett.*, 2021, **6**, 1920–1941.

3 S. P. Culver, A. G. Squires, N. Minafra, C. W. F. Armstrong, T. Krauskopf, F. Bocher, C. Li, B. J. Morgan and W. G. Zeier, Evidence for a Solid-Electrolyte Inductive Effect in the Superionic Conductor $Li_{10}Ge_{1-x}Sn_xP_2S_{12}$, *J. Am. Chem. Soc.*, 2020, **142**, 21210–21219.

4 N. Kamaya, K. Homma, Y. Yamakawa, M. Hirayama, R. Kanno, M. Yonemura, T. Kamiyama, Y. Kato, S. Hama, K. Kawamoto and A. Mitsui, A lithium superionic conductor, *Nat. Mater.*, 2011, **10**, 682–686.

5 T. Krauskopf, S. P. Culver and W. G. Zeier, Bottleneck of Diffusion and Inductive Effects in $Li_{10}Ge_{1-x}Sn_xP_2S_{12}$, *Chem. Mater.*, 2018, **30**, 1791–1798.

6 W. Xia, Y. Zhao, F. Zhao, K. Adair, R. Zhao, S. Li, R. Zou, Y. Zhao and X. Sun, Antiperovskite Electrolytes for Solid-State Batteries, *Chem. Rev.*, 2022, **122**, 3763–3819.

7 Y. Zhao and L. L. Daemen, Superionic conductivity in lithium-rich anti-perovskites, *J. Am. Chem. Soc.*, 2012, **134**, 15042–15047.

8 S. Stegmaier, J. Voss, K. Reuter and A. C. Luntz, $Li^+$ Defects in a Solid-State Li Ion Battery: Theoretical Insights with a $Li_3OCl$ Electrolyte, *Chem. Mater.*, 2017, **29**, 4330–4340.

9 J. A. Dawson, T. S. Attari, H. Chen, S. P. Emge, K. E. Johnston and M. S. Islam, Elucidating lithium-ion and proton dynamics in anti-perovskite solid electrolytes, *Energy Environ. Sci.*, 2018, **11**, 2993–3002.

10 Z. D. Hood, H. Wang, A. Samuthira Pandian, J. K. Keum and C. Liang, $Li_2OHCl$ Crystalline Electrolyte for Stable Metallic Lithium Anodes, *J. Am. Chem. Soc.*, 2016, **138**, 1768–1771.

11 Y. Li, W. Zhou, S. Xin, S. Li, J. Zhu, X. Lu, Z. Cui, Q. Jia, J. Zhou, Y. Zhao and J. B. Goodenough, Fluorine-Doped Antiperovskite Electrolyte for All-Solid-State Lithium-Ion Batteries, *Angew. Chem.*, 2016, **55**, 9965–9968.

12 G. Schwering, A. Honnerscheid, L. V. Wullen and M. Jansen, High lithium ionic conductivity in the lithium halide hydrates $Li_{3-n}(OH_n)Cl$ ($0.83 \leq n \leq 2$) and $Li_{3-n}(OH_n)Br$($1 \leq n \leq 2$) at ambient temperatures, *ChemPhysChem*, 2003, **4**, 343–348.

13 J. Howard, Z. D. Hood and N. A. W. Holzwarth, Fundamental aspects of the structural and electrolyte properties of $Li_2OHCl$ from simulations and experiment, *Phys. Rev. Mater.*, 2017, **1**, 075406.

14 A. Koedtruad, M. A. Patino, N. Ichikawa, D. Kan and Y. Shimakawa, Crystal structures and ionic conductivity in $Li_2OHX$ (X = Cl, Br) antiperovskites, *J. Solid State Chem.*, 2020, **286**, 121263.

15 A.-Y. Song, Y. Xiao, K. Turcheniuk, P. Upadhya, A. Ramanujapuram, J. Benson, A. Magasinski, M. Olguin, L. Meda, O. Borodin and G. Yushin, Protons Enhance Conductivities in Lithium Halide Hydroxide/Lithium Oxyhalide Solid Electrolytes by Forming Rotating Hydroxy Groups, *Adv. Energy Mater.*, 2018, **8**, 1700971.

16 Z. Deng, D. Ni, D. Chen, Y. Bian, S. Li, Z. Wang and Y. Zhao, Anti-perovskite Materials for Energy Storage Batteries, *InfoMat*, 2021.

17 G. Schwering, A. Honnerscheid, L. V. Wullen and M. Jansen, High lithium ionic conductivity in the lithium halide hydrates $Li_{3-n}(OH_n)Cl$ ($0.83 \leq n \leq 2$) and $Li_{3-n}(OH_n)Br$($1 \leq n \leq 2$) at ambient temperatures, *ChemPhysChem*, 2003, **4**, 343–348.

18 A. Y. Song, K. Turcheniuk, J. Leisen, Y. Xiao, L. Meda, O. Borodin and G. Yushin, Understanding Li-Ion Dynamics in Lithium Hydroxychloride ($Li_2OHCl$) Solid State Electrolyte via Addressing the Role of Protons, *Adv. Energy Mater.*, 2020, **10**, 1903480.

19 J. Zheng, B. Perry and Y. Wu, Antiperovskite Superionic Conductors: A Critical Review, *ACS Mater. Au*, 2021, **1**, 92–106.

20 M. B. Effat, J. Liu, Z. Lu, T. H. Wan, A. Curcio and F. Ciucci, Stability, Elastic Properties, and the Li Transport Mechanism of the Protonated and Fluorinated Antiperovskite Lithium Conductors, *ACS Appl. Mater. Interfaces*, 2020, **12**, 55011–55022.

21 Y.-S. Lee, S.-Y. Jung and K.-S. Ryu, Electrochemical Stability and Performance of $Li_2OHCl$ Substituted by F or Br as Solid-State Electrolyte, *J. Electrochem. Energy Convers. Storage*, 2021, **18**, 021011.

22 L. Yin, H. Yuan, L. Kong, Z. Lu and Y. Zhao, Engineering Frenkel defects of anti-perovskite solid-state electrolytes and their applications in all-solid-state lithium-ion batteries, *Chem. Commun.*, 2020, **56**, 1251–1254.

23 P. Hartwig and W. Weppneg, Ionic conductivities of Lithium-halide-based quateranry compounds, *Solid State Ionics*, 1981, **3**, 249–254.

24 J. Lee, B. Darminto, S. Narayanan, M. Diazlopez, A. W. Xiao, Y. Chart, J. H. Lee, J. A. Dawson and M. Pasta, Li-ion conductivity in $Li_2OHCl_{1−x}Br_x$ solid electrolytes: grains, grain boundaries and interfaces, *J. Mater. Chem. A*, 2022, **10**, 11574–11586.

25 G. Kresse and J. Hafner, Ab initio molecular dynamics for liquid metals, *Phys. Rev. B: Condens. Matter Mater. Phys.*, 1993, **47**, 558–561.

26 G. Kresse and J. Hafner, Ab initio molecular-dynamics simulation of the liquid-metal-amorphous-semiconductor transition in germanium, *Phys. Rev. B: Condens. Matter Mater. Phys.*, 1994, **49**, 14251–14269.

27 G. Kresse and J. Hafner, Ab initio molecular dynamics for open-shell transition metals, *Phys. Rev. B: Condens. Matter Mater. Phys.*, 1993, **48**, 13115–13118.

28 K. B. John, P. Perdew and M. Ernzerhof, Generalized Gradient Approximation Made Simple, *Phys. Rev. Lett.*, 1996, **77**, 3865–3868.

29 J. Heyd, G. E. Scuseria and M. Ernzerhof, Hybrid functionals based on a screened Coulomb potential, *J. Chem. Phys.*, 2003, **118**, 8207–8215.

30 S. P. Ong, W. D. Richards, A. Jain, G. Hautier, M. Kocher, S. Cholia, D. Gunter, V. L. Chevrier, K. A. Persson and G. Ceder, Python Materials Genomics (pymatgen): A robust, open-source python library for materials analysis, *Comput. Mater. Sci.*, 2013, **68**, 314–319.

31 H. Tang, Z. Deng, Z. Lin, Z. Wang, I.-H. Chu, C. Chen, Z. Zhu, C. Zheng and S. P. Ong, Probing Solid–Solid Interfacial Reactions in All-Solid-State Sodium-Ion Batteries with First-Principles Calculations, *Chem. Mater.*, 2017, **30**, 163–173.

32 Z. Deng, Z. Wang, I.-H. Chu, J. Luo and S. P. Ong, Elastic Properties of Alkali Superionic Conductor Electrolytes from First Principles Calculations, *J. Electrochem. Soc.*, 2015, **163**, A67–A74.

33 I. Hanghofer, G. J. Redhammer, S. Rohde, I. Hanzu, A. Senyshyn, H. M. R. Wilkening and D. Rettenwander, Untangling the Structure and Dynamics of Lithium-Rich Anti-Perovskites Envisaged as Solid Electrolytes for Batteries, *Chem. Mater.*, 2018, **30**, 8134–8144.

34 H. J. Lee, B. Darminto, S. Narayanan, M. Diaz-Lopez, A. W. Xiao, Y. Chart, J. H. Lee, J. A. Dawson and M. Pasta, Li-ion conductivity in $Li_2OHCl_{1−x}Br_x$ solid electrolytes: grains, grain boundaries and interfaces, *J. Mater. Chem. A*, 2022.

35 B. Zhang, Z. Lin, L. W. Wang and F. Pan, Achieving Both High Ionic Conductivity and High Interfacial Stability with the $Li_{2+x}C_{1-x}B_xO_3$ Solid-State Electrolyte: Design from Theoretical Calculations, *ACS Appl. Mater. Interfaces*, 2020, **12**, 6007–6014.

36 F. Wang, H. A. Evans, K. Kim, L. Yin, Y. Li, P.-C. Tsai, J. Liu, S. H. Lapidus, C. M. Brown, D. J. Siegel and Y.-M. Chiang, Dynamics of Hydroxyl Anions Promotes Lithium Ion Conduction in Antiperovskite $Li_2OHCl$, *Chem. Mater.*, 2020, **32**, 8481–8491.

37 W. D. Richards, L. J. Miara, Y. Wang, J. C. Kim and G. Ceder, Interface Stability in Solid-State Batteries, *Chem. Mater.*, 2015, **28**, 266–273.

38 R. Chen, Q. Li, X. Yu, L. Chen and H. Li, Approaching Practically Accessible Solid-State Batteries: Stability Issues Related to Solid Electrolytes and Interfaces, *Chem. Rev.*, 2020, **120**, 6820–6877.

39 X. Li, J. Liang, X. Yang, K. R. Adair, C. Wang, F. Zhao and X. Sun, Progress and perspectives on halide lithium conductors for all-solid-state lithium batteries, *Energy Environ. Sci.*, 2020, **13**, 1429–1461.

40 T. H. Wan and F. Ciucci, Electro-chemo-mechanical modeling of solid-state batteries, *Electrochim. Acta*, 2020, **331**, 135355.

41 J. Schnell, T. Günther, T. Knoche, C. Vieider, L. Köhler, A. Just, M. Keller, S. Passerini and G. Reinhart, All-solid-state lithium-ion and lithium metal batteries – paving the way to large-scale production, *J. Power Sources*, 2018, **382**, 160–175.

42 P. Pegolo, S. Baroni and F. Grasselli, Temperature- and vacancy-concentration-dependence of heat transport in $Li_3ClO$ from multi-method numerical simulations, *npj Comput. Mater.*, 2022, **8**.

43 S. Yu, R. D. Schmidt, R. Garcia-Mendez, E. Herbert, N. J. Dudney, J. B. Wolfenstine, J. Sakamoto and D. J. Siegel, Elastic Properties of the Solid Electrolyte $Li_7La_3Zr_2O_{12}$ (LLZO), *Chem. Mater.*, 2015, **28**, 197–206.

44 M. Yu and D. R. Trinkle, Accurate and efficient algorithm for Bader charge integration, *J. Chem. Phys.*, 2011, **134**, 064111.

45 N. Agmon, The Grotthuss mechanism, *Chem. Phys. Lett.*, 1995, **244**, 456–462.

46 K. Jun, Y. Sun, Y. Xiao, Y. Zeng, R. Kim, H. Kim, L. J. Miara, D. Im, Y. Wang and G. Ceder, Lithium superionic conductors with corner-sharing frameworks, *Nat. Mater.*, 2022, 924–931.

47 R. D. Shannon, Revised Effective Ionic Radii and Systematic Studies of Interatomie Distances in Halides and Chaleogenides, *Acta Crystallographica Section A*, 1976, **A32**, 751–754.

48 M. A. Kraft, S. Ohno, T. Zinkevich, R. Koerver, S. P. Culver, T. Fuchs, A. Senyshyn, S. Indris, B. J. Morgan and W. G. Zeier, Inducing High Ionic Conductivity in the Lithium Superionic Argyrodites $Li_{6+x}P_{1−x}Ge_xS_5I$ for All-Solid-State Batteries, *J. Am. Chem. Soc.*, 2018, **140**, 16330–16339.

49 S. Muy, R. Schlem, Y. Shao-Horn and W. G. Zeier, Phonon–Ion Interactions: Designing Ion Mobility Based on Lattice Dynamics, *Adv. Energy Mater.*, 2020, **11**, 2002787.

50 L. F. N. Zhizhen Zhang, Exploiting the paddle-wheel mechanism for the design of fast ion conductors, *Nat. Rev. Mater.*, 2022, **7**, 389–405.

51 K. E. Kweon, J. B. Varley, P. Shea, N. Adelstein, P. Mehta, T. W. Heo, T. J. Udovic, V. Stavila and B. C. Wood, Structural, Chemical, and Dynamical Frustration: Origins of Superionic Conductivity in closo-Borate Solid Electrolytes, *Chem. Mater.*, 2017, **29**, 9142–9153.

52 Y. Sun, Y. Wang, X. Liang, Y. Xia, L. Peng, H. Jia, H. Li, L. Bai, J. Feng, H. Jiang and J. Xie, Rotational Cluster Anion Enabling Superionic Conductivity in Sodium-Rich Antiperovskite $Na_3OBH_4$, *J. Am. Chem. Soc.*, 2019, **141**, 5640–5644.

53 Y. Sadikin, M. Brighi, P. Schouwink and R. Černý, Superionic Conduction of Sodium and Lithium in Anion-Mixed Hydroborates $Na_3BH_4B_{12}H_{12}$ and $(Li_{0.7}Na_{0.3})_3BH_4B_{12}H_{12}$, *Adv. Energy Mater.*, 2015, **5**, 1501016.

54 H. Fang and P. Jena, Argyrodite-type advanced lithium conductors and transport mechanisms beyond peddle-wheel effect, *Nat. Commun.*, 2022, **13**, 2078.

55 Y. Z. Sun, B. Ouyang, Y. Wang, Y. Q. Zhang, S. Sun, Z. Cai, V. Lacivita, Y. S. Guo and G. Ceder, Enhanced ionic conductivity and lack of paddle-wheel effect in pseudohalogen-substituted Li argyrodites, *Matter*, 2022, **5**, 1–17.

56 R. H. Chen, Z. M. Xu, Y. C. Lin, B. Y. Lv, S. H. Bo and H. Zhu, Influence of Structural Distortion and Lattice Dynamics on Li-Ion Diffusion in $Li_3OCl_{1-x}Br_x$ Superionic Conductors, *ACS Appl. Energy Mater.*, 2021, **4**, 2107–2114.